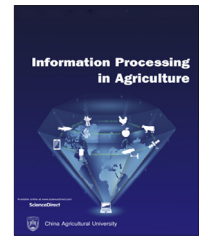


Available at www.sciencedirect.com

INFORMATION PROCESSING IN AGRICULTURE xxx (xxxx) xxx

journal homepage: www.elsevier.com/locate/inpa

Segmentation and measurement scheme for fish morphological features based on Mask R-CNN

Chuang Yu, Xiang Fan, Zhuhua Hu*, Xin Xia, Yaochi Zhao*, Ruqing Li, Yong Bai

School of Information and Communication Engineering, School of Computer Science and Cyberspace Security, Hainan University, Haikou 570228, China

ARTICLE INFO

Article history:

Received 4 June 2019

Received in revised form

5 January 2020

Accepted 13 January 2020

Available online xxxx

Keywords:

Mask R-CNN

Fish morphological feature

Image segmentation

Feature measurement

ABSTRACT

The morphological features of fish, such as the body length, the body width, the caudal peduncle length, the caudal peduncle width, the pupil diameter, and the eye diameter are very important indicators in smart mariculture. Therefore, the accurate measurement of the morphological features is of great significance. However, the existing measurement methods mainly rely on manual measurement, which is operationally complex, low efficiency, and high subjectivity. To address these issues, this paper proposes a scheme for segmenting fish image and measuring fish morphological features indicators based on Mask R-CNN. Firstly, the fish body images are acquired by a home-made image acquisition device. Then, the fish images are preprocessed and labeled, and fed into the Mask R-CNN for training. Finally, the trained model is used to segment fish image, thus the morphological features indicators of the fish can be obtained. The experimental results demonstrate that the proposed scheme can segment the fish body in pure and complex backgrounds with remarkable performance. In pure background, the average relative errors (AREs) of all indicators measured all are less than 2.8%, and the AREs of body length and body width are less than 0.8%. In complex background, the AREs of all indicators are less than 3%, and the AREs of body length and body width is less than 1.8%.

© 2020 China Agricultural University. Production and hosting by Elsevier B.V. on behalf of KeAi. This is an open access article under the CC BY-NC-ND license (<http://creativecommons.org/licenses/by-nc-nd/4.0/>).

1. Introduction

With the advancing of its scientific and technological capabilities, China has made great achievements in the mariculture. The production accounts for more than 70% of the world's overall mariculture output [1]. The measurement of body length, body width and other morphological features of fish have wide application prospects in smart mariculture. Due to

the difference in the quality and feeding ability of the Juvenile fish, the growth of the fish in the same pond is significantly different after a period of growth. Then, the fish needs to be classified. Grading can make fish grow better and improve feed utilization [2]. The fish body length and body width are closely related to the weight of the fish. In the mariculture, the fishermen judge the growth of the fish by collecting the morphological feature of the fish, and use the information as an important reference for feeding, fishing and classification [3]. At present, most of the measurement methods of fish body morphological features are manual, the operator uses measuring ruler to measure manually. It requires high technical level, and has high labor intensity and low efficiency. Furthermore,

* Corresponding authors.

E-mail addresses: eagler_hu@hainanu.edu.cn (Z. Hu), zhyc@hainanu.edu.cn (Y. Zhao).

Peer review under responsibility of China Agricultural University.
<https://doi.org/10.1016/j.inpa.2020.01.002>

2214-3173 © 2020 China Agricultural University. Production and hosting by Elsevier B.V. on behalf of KeAi.

This is an open access article under the CC BY-NC-ND license (<http://creativecommons.org/licenses/by-nc-nd/4.0/>).

the measurement result is subjectively affected, and the measurement takes a long time, which is easy to cause irreversible influence on the growth of the fish [4].

For measuring the fish body characteristics, some scholars have carried out certain research work in recent years. Image processing technology is widely used in quantitative analysis of fish features such as fish eyes, fish bodies, and caudal peduncles [5]. In the field of fish body feature detection, AdaBoost training method [6] and neural network method [7] are usually used to train fish body classifier to realize automatic detection of fish body. Yu et al. combined the machine vision and load cell technology to design a system that can automatically detect the quality, body length, and body width of large yellow croaker [8]. Zhang et al. applied machine vision technology to obtain the freshwater fish sample image, and pre-processed the sample image with grayscale, binarization and contour extraction to obtain the characteristic values such as the length axis and projection area, and established the length and quality relationship of the fish head, abdomen and caudal peduncle [9]. Hu et al. realized the automatic measurement of pupil diameter based on the intelligent measurement method of AdaBoost with weight constraint and improved Hough circle transformation. Besides, he measured the caudal peduncle length through corner point detection and least square linear fitting [10,11]. Wang proposed a Tri The-SIFT algorithm, a series of improvements to the SIFT algorithm, improved the descriptor accuracy and matching performance of the fish-eye image while maintaining the original robustness to scale and rotation [12]. Li et al. used the Canny operator to extract the fish body contour, and then calculated the body length and width of the fish for the classification of fish [13]. Azarmdel et al. developed a system for automatic processing of trout by using image processing algorithm, which can accurately segment fins and determine the optimal cutting point to achieve the optimal fish processing [14]. Issac et al. proposed a method of image segmentation based on region threshold. The method can effectively eliminate noise existing in the image, which only retains the image of fish gills [15]. Cook et al. employed imaging sonars to obtain the length characteristics of fish under low light, and the measurement effect is equivalent to the precision of other technologies [16]. At present, although the application of computer vision in fish body feature detection is extensive, it still cannot be applied with high precision for complex scenes. With the development of deep learning [17], Mask R-CNN has been proposed as an instance segmentation algorithm and it shows good performance for image segmentation and object identification [18].

To address the above problems, this paper proposes a method based on Mask R-CNN to segment and measure fish morphological features. Our proposed scheme can achieve automatic, accurate, and batch-efficient segmentation and measurement of fish morphological features. Our scheme has the following advantages.

- (1) The proposed scheme can resolve the problems of cumbersome manual operation and strong subjectivity, and avoid the impact of the measurement process on the normal growth of fish.

- (2) We build and publish a labeled sample set of oval squid online. The characteristic areas of the fish body can be accurately segmented, which is beneficial to the separate study of the parts of fish body.
- (3) The proposed scheme can obtain the accurate measurement precision and robustness under complex background.

The remainder of this paper is organized as follows. The data acquisition and the proposed scheme based on Mask R-CNN are introduced in Section 2. Section 3 describes experiment processes and analyzes the experimental results. Section 4 concludes this paper.

2. Data acquisition and proposed scheme

2.1. Data collection

The samples of oval squid (The Latin name is *Trachinotus ovatus*) used in the experiment is collected from the carp farm in Hainan Lingshui Autonomous County, China (Hainan University Marine College Aquaculture Professional Production and Research Base).

As shown in Fig. 1, we use a home-made image acquisition device to obtain the image of fish body. The device consists of a standard measuring plate (bottom length 560 mm, width 400 mm) and a mechanical arm. The process of collecting the fish body image is as follows. Firstly, the acquisition camera is (OLYMPUS TG-4, f/2.0, focal length: 4 mm, self-contained lens distortion correction) installed at the end of the execution of the mechanical arm, and use the data line to connect it with the computer. Next, the position of the camera is set by adjusting the robot arm so that the photographing screen can cover the bottom length of the platform, and the camera lens is parallel to the platform. Then, we place the fish on the measuring plate, keep the camera directly above the fish body, quickly capture the image, and collect the image data of the fish body to transmit to the computer through the data line.

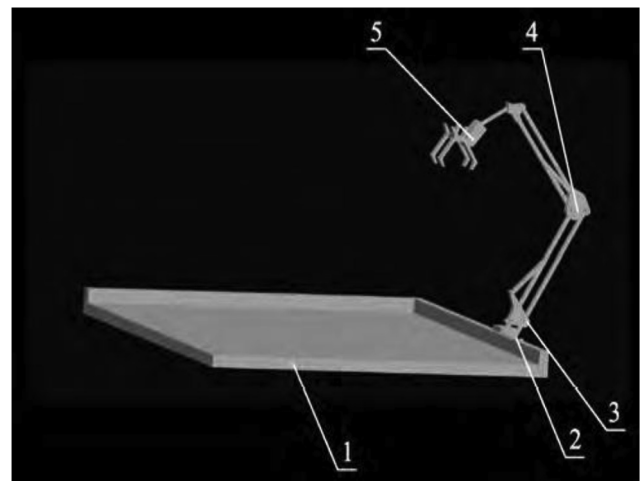


Fig. 1 – Image acquisition device.

Our collected data set is divided into simple data set (the image is collected from a simple background) and complex data set (from a complex background). Each data set contains 250 fish body images, respectively. In each data set, we randomly selected 200 images as the training set and the rest as the testing images. Especially, to improve the robustness of the algorithm to illumination and prevent the over fitting of the trained model, we argument each training set up to 400 by contrast adjustment [19]. We trained and tested the images on the two data sets, respectively.

Fig. 2 shows the required morphological indicators of the *Trachinotus ovatus* to be measured [20]. In Fig. 2, BL, BW, CPL, CPW, PD, and ED denote the body length, the body width, the caudal peduncle length, the caudal peduncle width, the pupil diameter, and the eye diameter, respectively. Specifically, BL refers to the longest distance of the fish body parallel to the horizontal direction. BW is the longest distance parallel to the vertical direction of the fish body except the dorsal and pelvic fins. The measurement of CPL and CPW is mainly based on the four turning points of the caudal peduncle. As shown in Fig. 2(a), we define these four turning points as A, B, C, and D. CPL refers to the longest distance of four points in the horizontal direction. CPW refers to the longest distance of four points in the vertical direction. The measurement of PD and ED is mainly based on the fact that the fish-eye and pupil of the fish sample in the pure background are approximately

round. PD refers to the longest distance parallel to the horizontal direction for the pupil. ED is the longest distance in the horizontal direction for the fish-eye.

2.2. The proposed segmentation and measurement scheme

2.2.1. Introduction to Mask R-CNN

Mask R-CNN is an algorithm that can perform target detection, target classification, and instance segmentation simultaneously in a neural network [21], which is an upgraded version of Faster R-CNN [22]. Compared to Faster R-CNN, Mask R-CNN has performance improvements in both time cost and accuracy. The algorithm implements pixel-level instance segmentation. Its structure is shown in Fig. 3.

The workflow of Mask R-CNN algorithm is as follows. Firstly, the images are input into a trained ResNext101 [23] and FPN [24] network to obtain the corresponding feature map [25]. ResNext101 is a convolutional neural network [26] that can improve the accuracy and reduce the number of hyperparameters without increasing the complexity of the parameters. Secondly, a fixed ROI [27] is preset for each point in the feature map, which typically sets a plurality of different fixed ratios to accommodate multiple shape recognitions. Thirdly, multiple ROIs are fed into RPN [28] in a binary classification [29] and Bounding-Box regression [30]. Binary

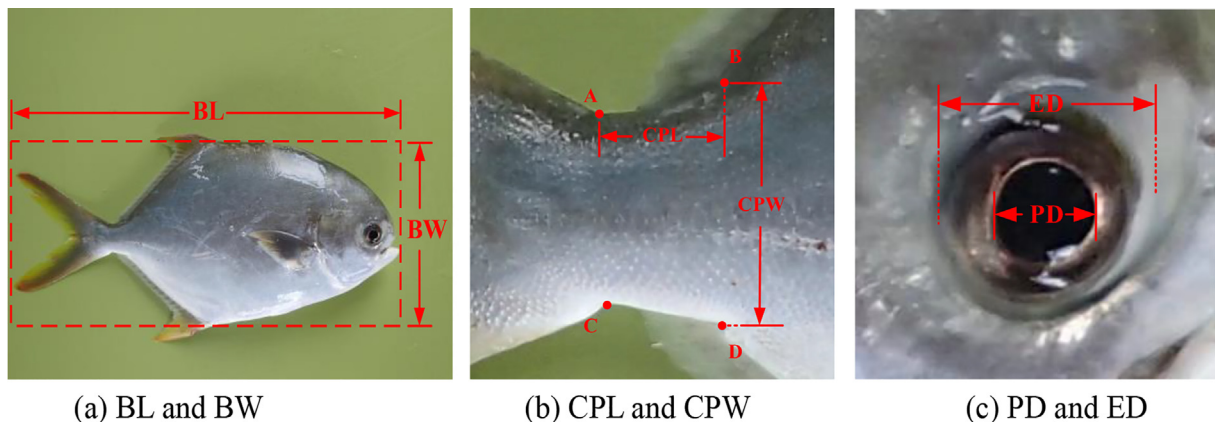


Fig. 2 – The morphological indicators to be detected.

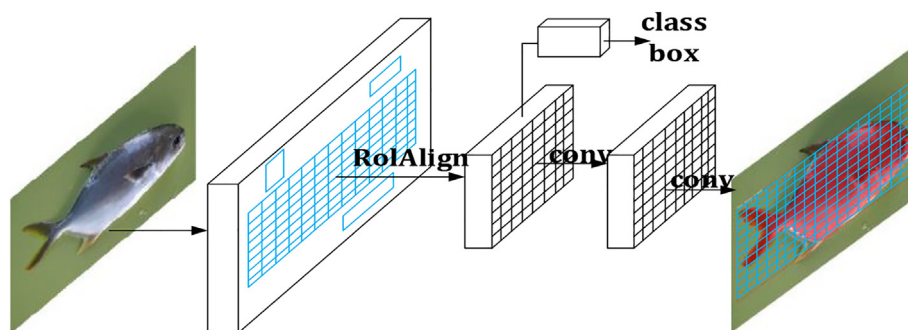


Fig. 3 – Flow chart of Mask R-CNN algorithm.

classification is used to distinguish the background and the target object to some extent. The Bounding-Box regression plays a regulatory role in approaching the real contour of the object. These two steps delete some unmatched ROIs. Finally, ROIAlign operation on the remaining ROIs is performed.

From Fig. 4, the method firstly traverses each candidate region, keeping the floating-point boundaries unquantized. Then, the candidate region is divided into $k \times k$ units, and the boundary result is not quantized. The fixed four coordinate positions are calculated in each unit. These four coordinates are the center positions of each quadrilateral after four

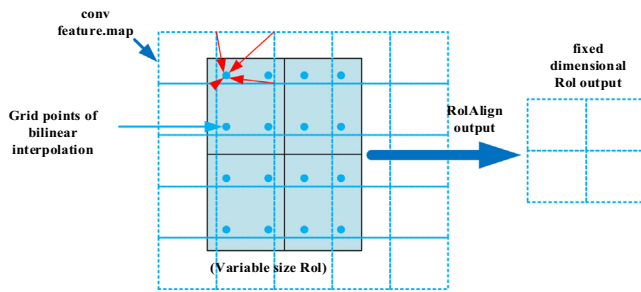


Fig. 4 – ROIAlign implementation diagram.

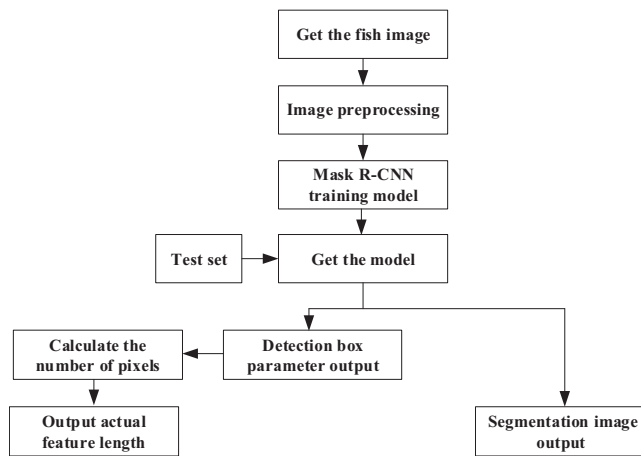


Fig. 5 – Flow chart of fish body morphological feature segmentation and measurement.

equal parts of the unit. The values of the four positions are calculated by bilinear interpolation method [31], and then the average or maximum values of the four positions are taken [32]. ROIAlign operation is an improvement on ROI Pooling [33]. Subsequently, the bilinear interpolation technique is used to eliminate the pixel offset caused by quantization in the feature extraction process of the backbone network. Such a step can reduce the deviation between the candidate box and the initial regression position achieving more accurate box out of the range. The rest of ROIs are performed by classification and Bounding-Box regression. Finally, the mask is generated by the FCN operation [34].

2.2.2. The proposed scheme based on Mask R-CNN

The morphological features of fish are segmented and measured based on Mask R-CNN. The overall flow chart is shown in Fig. 5.

As depicted in Fig. 5, the fish body image is first acquired through the image acquisition device, and then the acquired

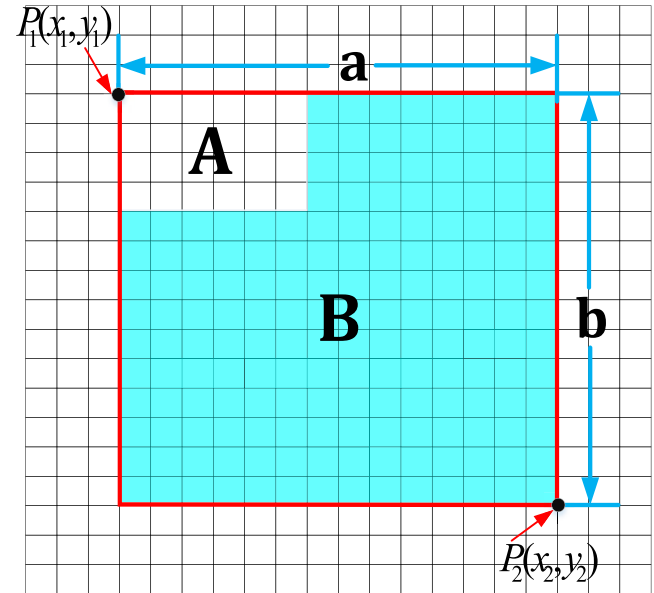


Fig. 7 – Schematic diagram of characteristic parameter measurement.

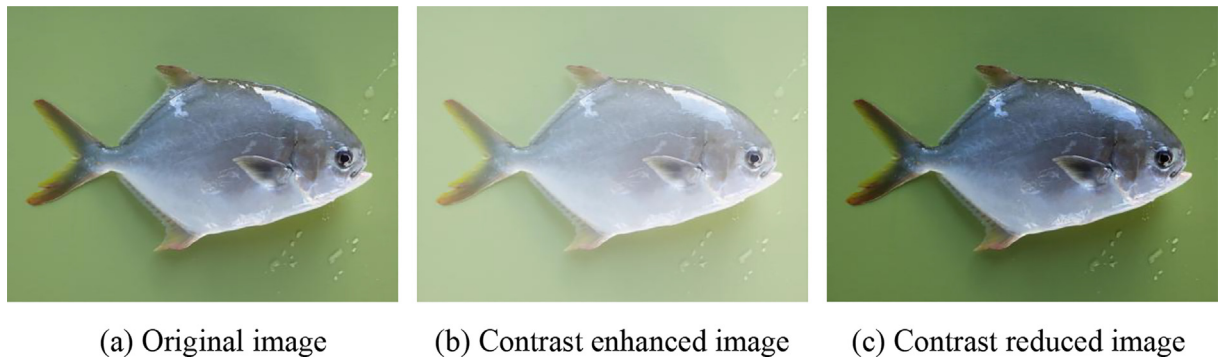


Fig. 6 – Original image and contrast changed images.

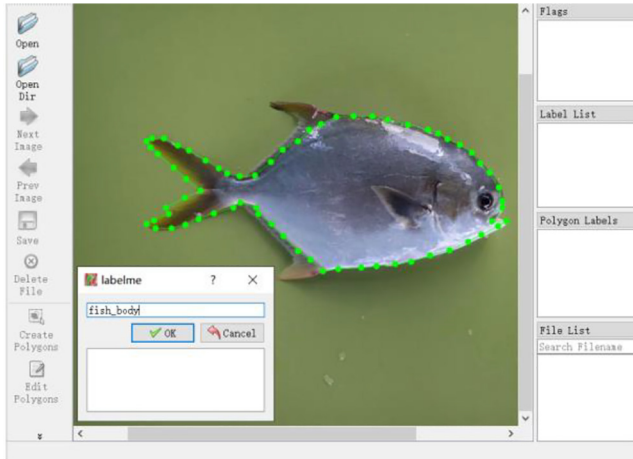


Fig. 8 – Fish body labeling.



Fig. 9 – Partial training sample diagram.

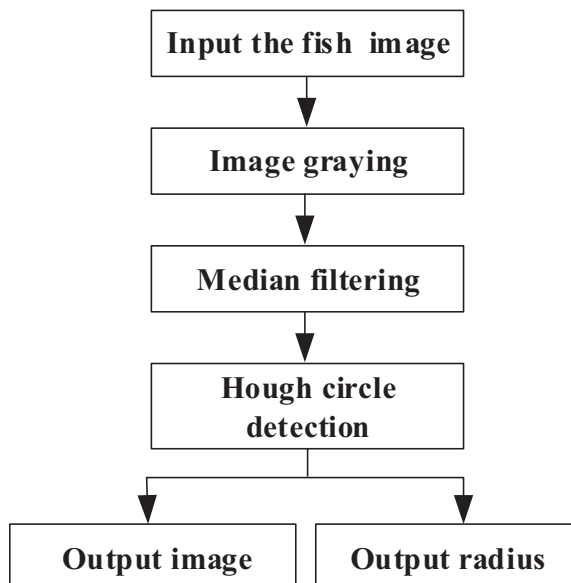


Fig. 10 – The detection flow chart of Hough circle algorithm.

image is preprocessed. In the preprocessing process, the contrast adjustment technique is used. In the experiments, we performed a contrast enhancement operation on 100 images and a contrast reduction operation on 100 images. The preprocessing effect is shown in Fig. 6. After such operations, the data set is augmented, and the influence of light and shade on detection is reduced, which enhances the robustness of the trained model. Then, the data set is annotated to construct a training set, which is fed into the Mask R-CNN network for training to obtain the trained model. After that, the test set is input into the trained model to obtain the segmented image and the relevant parameters of the target frame. Finally, the final result is obtained by calculating the number of pixels in the detection frame and mapping to the actual fish feature parameters.

Fig. 7 is a schematic diagram of measurement of characteristic parameters. Each small grid in the figure denotes a pixel point. The region A and region B represent the total region of the detection box and the segmented object region, respectively. $p_1(x_1, y_1)$ and $p_2(x_2, y_2)$ represent the coordinate of the upper left point and the coordinate of the upper right point of the detection frame, respectively. a and b denote the number of pixels in the length and width of the detection frame, respectively.

To obtain the values of PD, FD, BL, BW, CPL and CPW, we use (1) to calculate the ratio of the actual length of the photo area (560 mm) to the number of pixels on the corresponding side of the photo. Then, using the trained model, an accurate recognition frame (as shown in Fig. 7) is generated for each segmented feature area. By obtaining the coordinates of the upper left point and the lower right point of the recognition frame, the length and width pixels of the recognition frame are calculated using (2) and (3). Finally, the actual length can be obtained by multiplying the number of calculated pixel points by θ using (4) and (5).

$$\theta = \frac{L}{n} \quad (1)$$

$$a = x_1 - x_2 \quad (2)$$

$$b = y_1 - y_2 \quad (3)$$

$$L_{real} = a \times \theta \quad (4)$$

$$W_{real} = b \times \theta \quad (5)$$

where L represents the actual length of the photo area, n represents the number of pixels in the image length, L_{real} represents the calculated length mapped to the actual length, W_{real} represents the calculated width mapped to the actual width.

3. Experiment and results analysis

3.1. Experimental setups and evaluation metrics

Our training setups are ubuntu18.04.1 operation system, Tesla v100 GPU, Tensorflow platform and Python3. Our test setups are Windows10 operation system, TITAN XP GPU, Intel(R) Core(TM) i7-7800x CPU @ 3.5GHZ, Tensorflow platform and Python3.

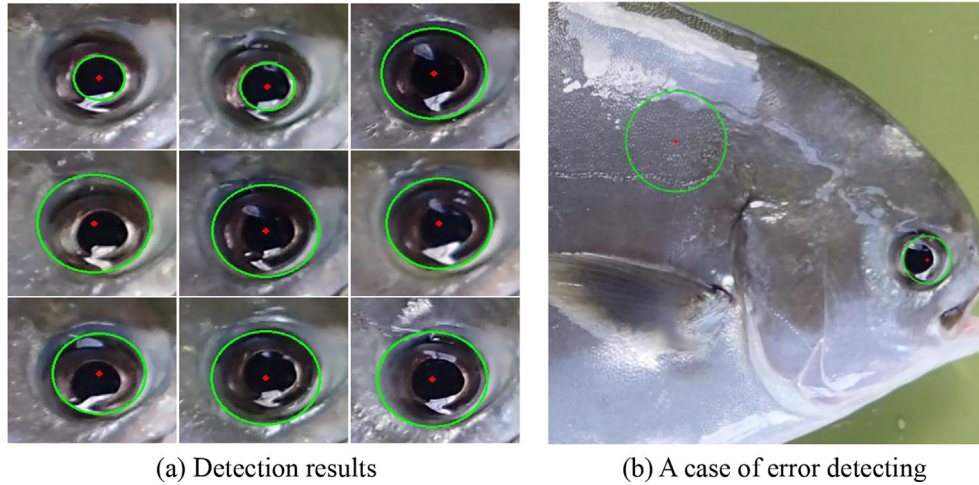


Fig. 11 – Detection results using the Hough circle algorithm.

In order to describe the effect of the test, we employ the relative error [35] and the average relative error [36] as the evaluation metrics. In order to obtain the PD, FD, BL, BW, CPL and CPW standard values of the test set, the fish in the test set were measured manually three times, and the average value was taken as the standard values. The manual measurement process is as follows. First, the fish is anesthetized, and then it is placed flat on the measuring fish plate. Finally, the technician uses the caliper to perform three independent measurements.

3.2. Generation of training sample set

The training sample set is used as the input of model training, which largely determines the quality of the training model. The proposed segmentation scheme is to obtain the

optimal segmentation effect by learning the input training sample set and continuously correcting the model. For the generation of the training sample set, the sample set is labeled by the *labelme* software in the experiment. Taking the fish body as an example, the schematic diagram of the annotation and some training sample set are shown in Figs. 8 and 9 (the complete training sample set has been uploaded with the code).

3.3. Segmentation and measurement under pure background

3.3.1. Segmentation and measurement of pupil and fish-eye

- (1) Detection of pupil and fish-eye based on traditional Hough circle algorithm



Fig. 12 – Fish's pupil segmentation.

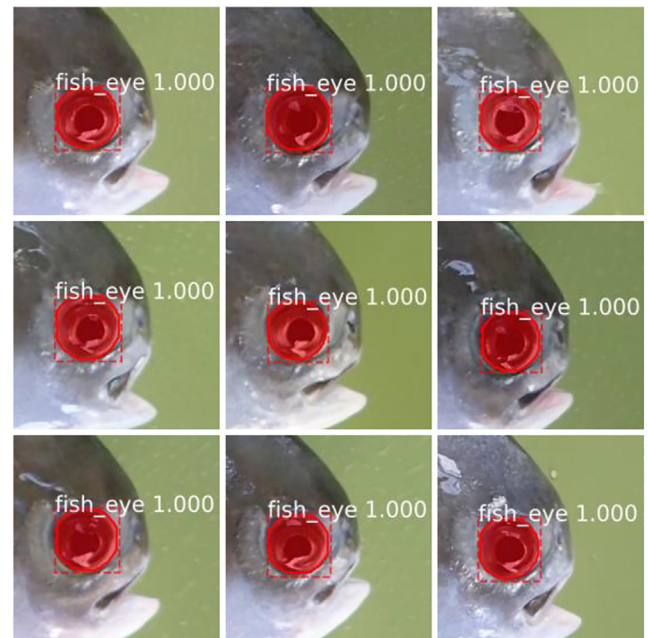


Fig. 13 – Fish-eye segmentation.

The Hough transform [37] is a boundary shape description method that is later extended to identify the detection circle. The detection process of the Hough circle algorithm is shown in Fig. 10.

As shown in Fig. 10, we firstly perform grayscale processing on the input image, and then perform median filtering [38] on the grayscale image. Finally, the relevant parameters of the Hough circle detection are adjusted to determine the optimal detection effect for output. Ten fish test images in a pure background are tested by using the traditional Hough circle method. By adjusting the parameters multiple times, the final test results are shown in Fig. 11. In order to well present the experimental results, the fish-eye region of the detected image is separately cropped.

From Fig. 11, the conventional Hough circle algorithm regions cannot accurately distinguish the pupil and eye regions, and the detection effect is poor. Moreover, there are many cases where there is a significant deviation of the detection area. Among the test results, there is a result image that detects the body part of the fish. The Hough circle algorithm requires mapping each point of the two-dimensional image space to the three-dimensional parameter space. It takes a lot of traversal to find the center of the circle and the radius. There is a large error in solving the parameters in an irregular circle.

(2) Segmentation and measurement of pupil and fish-eye based on Mask R-CNN

When using the scheme proposed in this paper to segment the fish-eye and pupil, the workflow is roughly as follows. Firstly, the preprocessed image is labeled to obtain two training sample sets of fish-eye and pupil. Then, the training sample set is input to the Mask R-CNN training model, the model is continuously optimized by iteratively learning and optimizing the weights during the training process. The continuous training process allows the model to better segment the fish-eye or pupil from the fish images. Finally, the test set is segmented for pupil and fish-eye experiments using a trained model. The partial experimental results are shown in Figs. 12 and 13. In order to well present the results, the pupil and fish-eye regions of the detected images are separately cropped.

From Figs. 12 and 13, the proposed method achieves better accuracy and robustness than the traditional Hough circle detection method. The proposed scheme can better segment the details of the feature area. In order to accurately display the experimental results, the calculated PD, ED and actual relative errors are shown in Figs. 14 and 15.

In the experiments, the pure fish test set is fed into the trained model for detecting PD and ED respectively. The

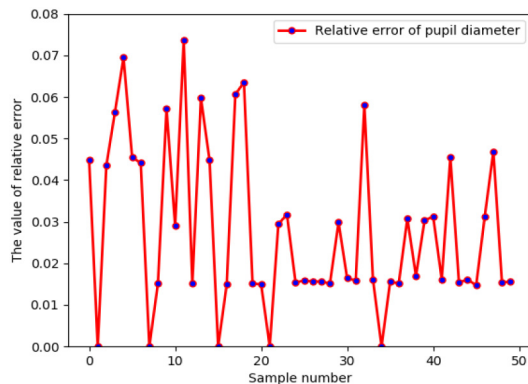


Fig. 14 – The relative error of PD.

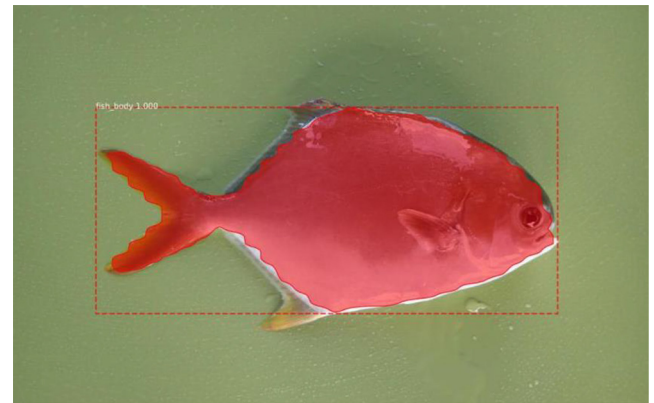


Fig. 16 – The output image after fish body segmentation.

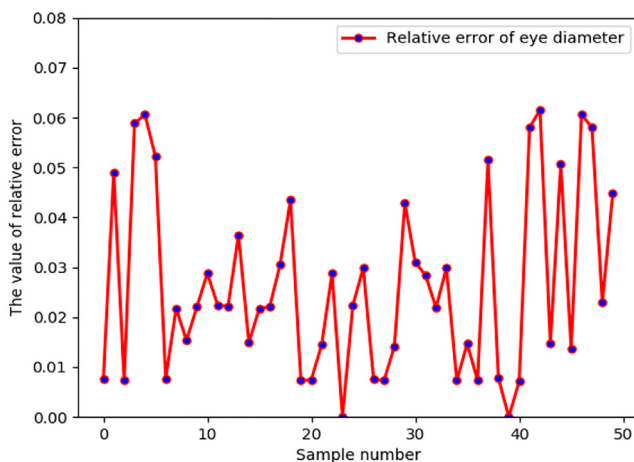


Fig. 15 – The relative error of ED.

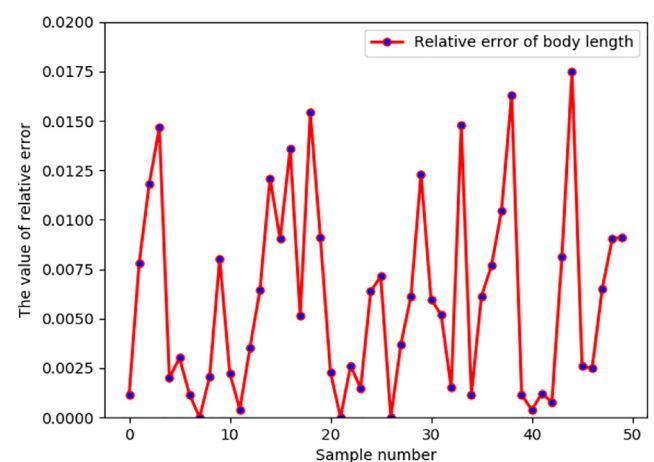


Fig. 17 – The relative error of BL.

relative error between the actual diameter and the measured value of each fish is calculated. From Figs. 14 and 15, the maximum relative errors of PD and ED are less than 0.08 and 0.07, respectively. By calculating the average of the relative errors, the average relative error of PD is 2.8%, and the average relative error of ED is 2.64%. Compared with the measurement results of the proposed scheme, the relative error in measuring the PD of the data set using the improved Hough circle transformation in [10] is 6.5%. Therefore, our proposed scheme achieves higher accuracy for the measurements of PD and ED under pure background.

3.3.2. Segmentation and measurement of fish body

BL and BW are important indicators for fishermen to judge the growth of fish. For the test set images, the trained model is used to obtain the segmented output images. The experimental results are shown in Fig. 16.

From Fig. 16, the length and width of the detection frame almost coincide with the BL and BW of the fish body to be detected. To verify the effect of the test numerically, we calculate the relative error of BL and BW in 50 test images respectively. The results are shown in Figs. 17 and 18.

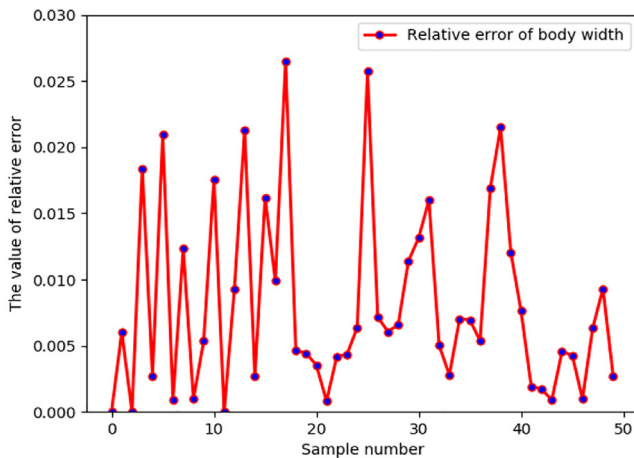


Fig. 18 – The relative error of BW.



Fig. 19 – The output image after caudal peduncle segmentation.

In the experiments, the pure fish test set is fed into the trained model for detecting BL and BW respectively. The relative error between the actual length and the measured value of each fish is calculated. From Fig. 17, Fig. 18, the maximum relative errors of BL and BW are less than 0.018 and 0.027 respectively. By calculating the average relative error, the average relative error of BL is 0.6%, and the average relative error of BW is 0.8%. It can be seen that the trained model is very accurate for BL and BW measurements under the pure background.

3.3.3. Segmentation and measurement of the caudal peduncle

The measurement of CPL and CPW is of great significance for the cultivation of fish. On the one hand, there is a significant correlation between the values of CPL and CPW and the body weight of fish, which can be one of the important indicators for breeding considerations. On the other hand, technician can identify fish with significant characteristics through CPL and CPW values, and the values of CPL and CPW can provide a data basis for fish genetic improvement services. For the test set images, the trained model is used to obtain the

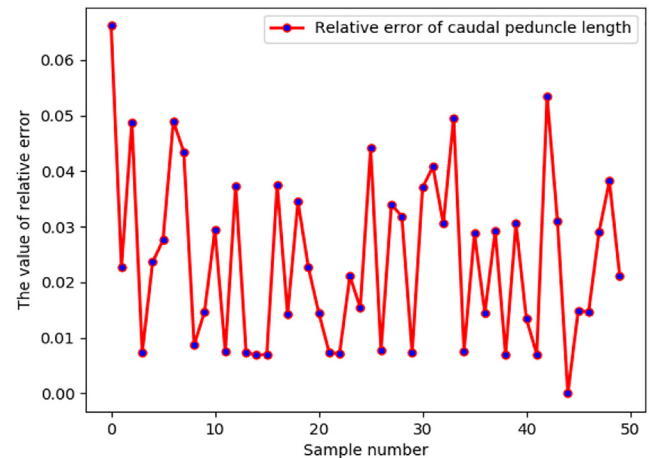


Fig. 20 – The relative error of CPL.

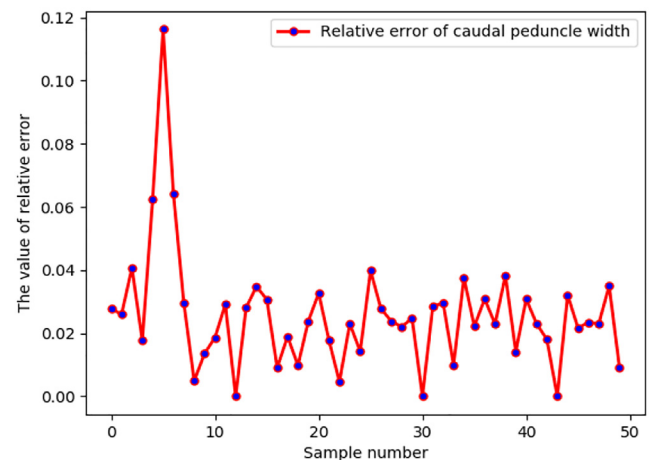


Fig. 21 – The relative error of CPW.

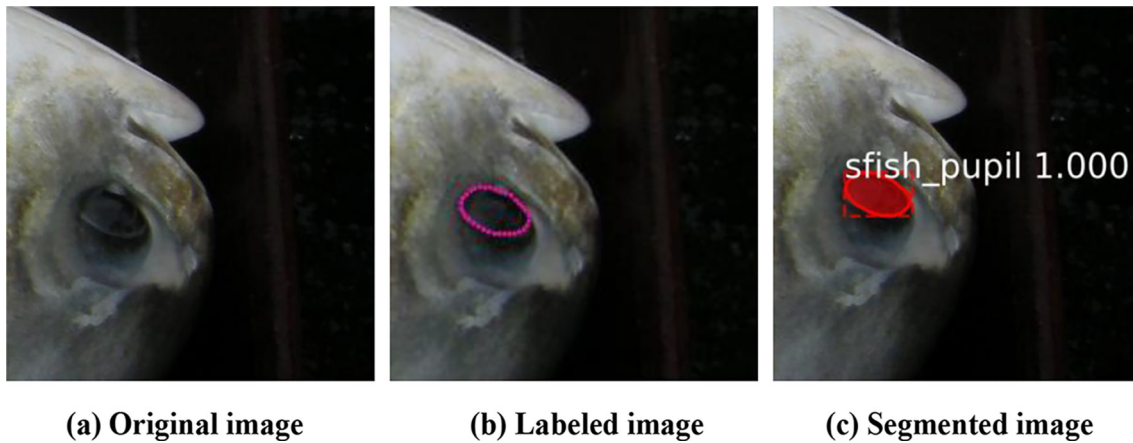


Fig. 22 – Fish's pupil area and segmentation effect.

segmented output images. The experimental results are shown in Fig. 19.

From Fig. 19, the output image is better segmented into the caudal peduncle region of the fish. The relative errors of the CPL and the CPW are shown in Figs. 20 and 21.

In the experiments, the pure fish test set is fed into the trained model for detecting CPL and CPW respectively. The relative error between the actual length and the measured value of each fish is calculated. As can be seen from Figs. 20 and 21, the overall measurement effect of the model on CPL and CPW is very good, but there are individual errors. The reason of the errors is that the inflection point of individual caudal peduncle is not obvious. The maximum relative errors of CPL and CPW are less than 0.07 and 0.12 respectively. The average relative error of CPL is 2.41%, and the average relative error of CPW is

2.57%. Compared with the measurement results of our proposed scheme, a caudal peduncle measurement method [11] based on image processing and linear fitting achieves 5% average relative error for CPL of the data set. Therefore, our proposed scheme has higher measurement accuracy for CPL and CPW.

3.4. Segmentation and measurement under complex background

In addition to the morphological feature segmentation and measurement of fish in pure background, we also segment and measure the morphological features of fish under complex background. The training and detection process in the complex background is consistent with the operation flow in the pure background.

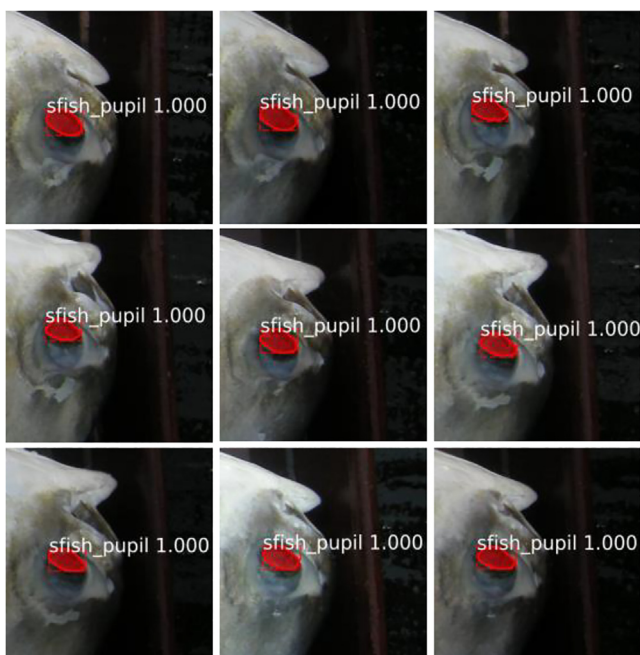


Fig. 23 – Output pupil images.

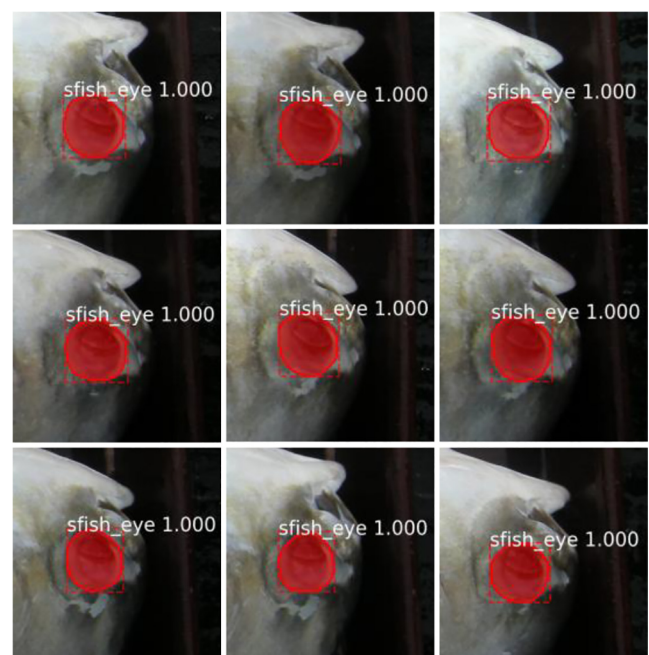


Fig. 24 – Output fish-eye images.

3.4.1. Segmentation and measurement of pupil and fish-eye
The other group of the experimental fish has a special pupil area, which is an irregular elliptical shape and cannot be nearly round, so the PD of the fish is not solved. From Fig. 22, the proposed scheme based on Mask R-CNN can accurately segment the irregular regions of the pupil to avoid the detection error caused by the shape.

The pupils and fish-eyes in the test set images are segmented by using the trained model, and the corresponding regions of the segmented image are cropped for better rendering.

As shown in Figs. 23 and 24, since the fish's pupil is irregular in shape, the fish-eye is also irregularly rounded. The experimental results show that the trained model can well segment the feature details and improve the measurement accuracy. By calculating the average relative error of the eye diameter under a complex background, the average relative error of ED is 2.8%.

3.4.2. Segmentation and measurement of fish body and caudal peduncle

We use the trained model to segment the fish body and the caudal peduncle under a complex background. The results of the experiments are shown in Figs. 25 and 26.

From Figs. 25 and 26, the morphological features of the test fish are all accurately segmented, and the detection frame is used to accurately capture the fish's characteristics. By calculating the relative error of the corresponding feature parameters of the test set and making statistics, the average relative error of BL under complex background is 1.29%, and the average relative error of BW is 1.71%. The average relative error of CPL is 2.93%, and the average relative error of CPW is 2.87%. Therefore, our proposed scheme can accurately segment and measure the fish body and caudal peduncle area under complex background. Its accuracy is similar to that of a pure background. Compared with our proposed scheme, the method proposed in [10] and [11] cannot measure the corresponding features for samples in complex background. Therefore, the proposed scheme can achieve better accuracy and have higher robustness.

3.5. Result comparisons between pure and complex background

We compute the max relative error (MaRE), the min relative error (MiRE) and the average relative error (ARE) in pure background (PB) and complex background (CB), respectively. Since the pupils of fish samples under complex background are

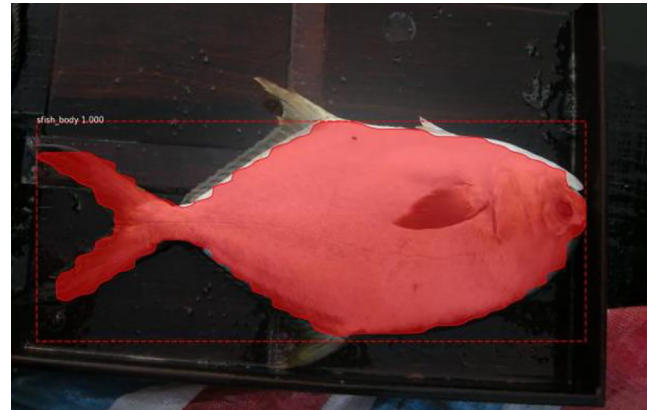


Fig. 25 – Fish body segmentation.



Fig. 26 – Caudal peduncle segmentation.

irregular oval, the PD values are meaningless. The comparison is shown in Table 1.

From Table 1, on the one hand, the average errors of each fish body features under different backgrounds are less than 3%, which indicates the proposed scheme has good performance. On the other hand, the average errors of fish body features under pure background are slightly better than that of complex background, which demonstrates that the complex environment indeed affects the detection accuracy to a certain extent, and it also shows that the proposed scheme has good robustness.

In addition, for complex and pure backgrounds, we analyze the data given in Table 1. First of all, because the fish

Table 1 – Results comparisons between pure background and complex background.

Features	MaRE in PB (%)	MaRE in CB (%)	MiRE in PB (%)	MiRE in CB (%)	ARE in PB (%)	ARE in CB (%)
BL	1.75	4.2	0	0.03	0.6	1.29
BW	2.65	5.47	0	0.09	0.8	1.71
CPL	6.62	6.41	0	0	2.41	2.93
CPW	11.63	10.53	0	0	2.57	2.87
ED	6.15	6.62	0	0	2.64	2.8
PD	7.35	–	0	–	2.8	–

eye in the image does not have direct contact with the background, its detection effect is less affected by the background. Therefore, under the CB and the PB, the difference of ARE index of ED feature is the least. Secondly, because the length of the fish's body length and body width are larger than CPL and CPW, the ARE of BL and BW are relatively small in both backgrounds. Finally, because the four intersections of some fish caudal peduncles are not clear enough, the error of the detection results will become large. Obviously, the MaRE of CPL and CPW in both backgrounds is relatively larger than that of several other fish morphology characteristics.

4. Conclusions

The morphological feature measurement of fish has been widely used in smart mariculture. This paper proposes a morphological feature segmentation and measurement scheme based on Mask R-CNN, which can detect various morphological features of fish. Firstly, the fish images are collected through the self-designed image acquisition device, and are transmitted to the computer. Next, the images are preprocessed by contrast adjustment to augment the data set while increasing robustness. Then, the labeled training set is trained by using the Mask R-CNN algorithm. Subsequently, the trained model is used to perform feature segmentation and output the results on the test set. Finally, we can obtain the measured values by mapping calculation.

From the experimental results, the proposed scheme can achieve high accuracy and robustness on the segmentation and measurement of the fish morphological feature in different backgrounds. The average relative error for PD, ED, BL, BW, CPL and CPW is less than 3%. The average relative error of BL and BW is only less than 1.8%.

Although we have obtained good results, there are still some rooms for improvement. In order to achieve convenient and efficient image capture of fish, we will design an automatic pipeline image acquisition device. In the future, we will implement an intelligent machine system through the segmentation and measurement scheme proposed in this paper.

Declaration of Competing Interest

The authors declared that there is no conflict of interest.

Acknowledgement

This research was supported by the National Natural Science Foundation of China (61963012, 61961014), the Natural Science Foundation of Hainan Province, China (619QN195, 618QN218); the Key R & D Project of Hainan Province, China (ZDYF2018015), and Collaborative Innovation Fund Project of Tianjin University-Hainan University (HDTDU201907).

Appendix A

The code and supplementary data associated with this article can be found, in the online version, at <https://github.com/Wahaha1314/Fish-characteristic-measurement>. (DOI: <https://doi.org/10.5281/zenodo.3472318>).

REFERENCES

- [1] Wang DF, Wang YT, Yang ZJ, Zhu ZW. Research and thinking on the multi-functionality of fisheries in China (Series 1). *China Fisheries* 2012;01:15–7.
- [2] Guo XY. The research of farmed fish grading system based on DSP. Tianjin University of Technology; 2016.
- [3] An AQ, Yu ZT, Wang HQ, Nie YF. Application of machine vision technique in agriculture machine. *J Anhui Agric Sci* 2007;12:3748–9.
- [4] Khammi A, Kutako M, Sangwichien C, Nootong K. Development and evaluation of compact aquaculture system for the application of zero water-exchange inland aquacultures. *Eng J* 2015;19:15–27.
- [5] Duan YE, Li DL, Li ZB, Fu ZT. Review on visual characteristic measurement research of aquatic animals based on computer vision. *Trans Chin Soc Agric Eng* 2015;31:1–11.
- [6] Benson B, Cho J, Goshorn D, Kastner R. Field Programmable Gate Array (FPGA) based fish detection using haar classifiers. Atlanta: American Academy of Underwater Sciences; 2009.
- [7] Alsmadi M, Omar K, Noah SAM, Almarashdeh I. Fish recognition based on robust features extraction from size and shape measurements using neural network. *J Comput Sci* 2010;6:1088–94.
- [8] Yu XJ, Wu XF, Wang JP, Chen L, Wang L. Rapid detecting method for *Pseudosciaena Crocea* morphological parameters based on the machine vision. *J Integration Technol* 2014;5:45–51.
- [9] Zhang ZQ, Niu ZY, Zhao SM, Yu JJ. Weight grading of freshwater fish based on computer vision. *J Agric Eng* 2011;27:350–4.
- [10] Hu ZH, Zhang YR, Zhao YC, Cao L, Huang MX, Bai Y. Fish eye recognition based on weighted constraint AdaBoost and pupil diameter automatic measurement with improved Hough circle transform. *Trans Chin Soc Agric Eng* 2017;23:226–32.
- [11] Hu ZH, Cao L, Zhang YR, Zhao YC. Study on fish caudal peduncle measuring method based on image processing and linear fitting. *Fishery Modernization* 2017;44(2):43–9.
- [12] Wang ED, Jiao JL, Yang JC, Liang DY, Tian JD. Tri-SIFT: A triangulation-based detection and matching algorithm for fish-eye images. *Information (Switzerland)* 2018;9:12.
- [13] Li L, Guo XY. Research on fish classification method based on image processing. *J Inner Mongolia Agric Univ (Nat Sci Ed)* 2015;36(5):120–4.
- [14] Azarmdel H, Mohtasebi SS, Ali J, Muñozb AR. Developing an orientation and cutting point determination algorithm for a trout fish processing system using machine vision. *Comput Electron Agric* 2019;162:613–29.
- [15] Issac A, Dutta MK, Sarkar B. Computer vision based method for quality and freshness check for fish from segmented gills. *Comput Electron Agric* 2017;139:10–21.
- [16] Cook D, Middlemiss K, Jaksons P, Davison W, Jerrett A. Validation of fish length estimations from a high frequency multi-beam sonar (ARIS) and its utilisation as a field-based measurement technique. *Fish Res* 2019;218:59–68.
- [17] Garcia-Garcia A, Orts-Escolano S, Oprea S, Villena-Martinez V, Martinez-Gonzalez P, Garcia-Rodriguez J. A survey on deep learning techniques for image and video semantic segmentation. *Appl Soft Comput* 2018;70:41–65.
- [18] He KM, Gkioxari G, Dollar P, Girshick R. Mask R-CNN. *IEEE Trans Pattern Anal Mach Intell* 2018.
- [19] Matsumoto M. Cognition-based contrast adjustment using neural network based face recognition system. In: *IEEE International Symposium on Industrial Electronics*; 2010. p. 3590–94.

- [20] Hu XL, Chen QY, Shen J. Study on morphological characteristics and correlation analysis of *Trachurus japonicus* from Southern East China Sea. *Acta Zootaxonomica Sinica* 2013;02(5):407–4122.
- [21] Chen H, Qi XJ, Yu LQ, Dou Q, Qin J, Heng P-A. DCAN: Deep contour-aware networks for object instance segmentation from histology images. *Med Image Anal* 2017;36:135–46.
- [22] Ren XQ, He KM, Girshick R, Sun J. Faster R-CNN: Towards real-time object detection with region proposal networks. *IEEE Trans Pattern Anal Mach Intell* 2017;39:1137–49.
- [23] He KM, Zhang XY, Ren SQ, Sun J. Deep residual learning for image recognition. In: 29th IEEE Conference on Computer Vision and Pattern Recognition; 2016. p. 770–778.
- [24] Liang ZW, Shao J, Zhang DY, Gao LL. Small object detection using deep feature pyramid networks. In: 19th Pacific-Rim Conference on Multimedia; 2018. p. 554–564.
- [25] Zhang ZL, Sun SH. Image fusion based on the self-organizing feature map neural networks. *Chin J Electron* 2001;10:96–9.
- [26] Girshick R, Donahue J, Darrell T, Malik J. Rich feature hierarchies for accurate object detection and semantic segmentation. In: IEEE Computer Society Conference on Computer Vision and Pattern Recognition; 2014. p. 580–587.
- [27] Vlahakis V, Kitney RI. ROI approach to wavelet-based, hybrid compression of MR images. In: 6th International Conference on Image Processing; 1997, 443, 833–837.
- [28] Yang B, Yan JJ, Lei Z, Li SZ. CRAFT objects from images. In: 29th IEEE Conference on Computer Vision and Pattern Recognition; 2016. p. 6043–6051.
- [29] Rahman A, Smith DV, Little B, Ingham AB, Greenwood PL, Bishop-Hurley GJ. Cattle behaviour classification from collar, halter, and ear tag sensors. *Inform Process Agric* 2018;5(1):124–33.
- [30] Mbelwa JT, Zhao QJ, Lu Y, Wang FS, Mbise M. Visual tracking using objectness-bounding box regression and correlation filters. *J Electron Imaging* 2018;27:2.
- [31] Wang HJ, Wang JL, Wang MH, Yin YM. Efficient image inpainting based on bilinear interpolation downscaling. *Opt Precision Eng* 2010;18:1234–41.
- [32] Xie B, Zhang HK, Xue J. Deep convolutional neural network for mapping smallholder agriculture using high spatial resolution satellite image. *Sensors* 2019;19(10):2398.
- [33] Yan C, Chen WH, Chen PCY, Kendrick AS, Wu XM. A new two-stage object detection network without RoI-Pooling. In: 30th Chinese Control and Decision Conference; 2018. p. 1680–1685.
- [34] Chen GZ, Zhang XD, Wang Q, Dai F, Gong YF, Zhu K. Symmetrical dense-shortcut deep fully convolutional networks for semantic segmentation of very-high-resolution remote sensing images. *IEEE J Sel Top Appl Earth Obs Remote Sens* 2018;11:1633–44.
- [35] Long SS, Zeng SQ, Gan SS, Xiao HS, Liu X, Xiang BW. Age estimation method II of uneven-aged forest based on the data of multistage diameter measurement. *J Central South Univ Forestry Technol* 2019;06:23–9.
- [36] Long XQ, Li J, Metro Chen YR. Short-term traffic flow prediction with deep learning. *Control Decision* 2018:1–14.
- [37] He YM, Dai SG. An algorithm for improving the precision of detecting round object by Hough Transform. *Microcomput Inform* 2009;25(10):279–81.
- [38] Momin MA, Rahman MT, Sultana MS, Igathinathane C, Ziauddinane ATM, Grift TE. Geometry-base mass grading of mango fruits using image processing. *Inform Process Agric* 2017;4(2):150–60.